KEC Conference 2026

ISSN: 3021-940X (Print) DOI:10.3126/injet.v3i2.95499

3D Frequency-Difference Electrical Impedance Tomography for Early Subcutaneous Edema Detection Using Tikhonov Regularization and Physics-Informed Neural Networks

Anish Maharjan[1], Sanjeeb Prasad Panday[2*], Lok Nath Regmi[3]

[1]*Department of Electronics and Computer Engineering, Pulchowk Campus, Tribhuvan University, Lalitpur, Nepal*
080mscsk003.anish@pcampus.edu.np
[2]*Department of Electronics and Computer Engineering, Pulchowk Campus, Tribhuvan University, Lalitpur, Nepal*
sanjeeb.panday@pcampus.edu.np
[3]*Department of Electronics and Computer Engineering, Pulchowk Campus, Tribhuvan University, Lalitpur, Nepal*
lnregmi046@pcampus.edu.np

Abstract

Subcutaneous edema is difficult to detect at an early stage because the associated conductivity changes are subtle and hard to localize using conventional imaging methods. This study presents the 3D Frequency Difference-Electrical Impedance Tomography (FD-EIT) framework for the detection of early-stage edema in the lower leg region. A 3D lower-leg model with 16 electrodes was simulated, and the boundary voltages and differential measurements were generated under a broader set of synthetic edema scenarios representing varied anomaly extent, irregularity, conductivity, contrast, and measurement difficulty. Reconstruction was evaluated using two approaches: the baseline method using Tikhonov regularization and the Physics-Informed Neural Network (PINN) method. The results show that the baseline method produces stable but spatially diffuse reconstructions, whereas the PINN method provides more localized and structured anomaly patterns that are aligned more closely with the ground-truth edema regions. Quantitative evaluation with RMSE, MAE, relative error, and Dice score showed better reconstruction accuracy and edema-mask localization for the PINN compared to the baseline method. However, the results should be interpreted as a controlled synthetic proof-of-concept because the PINN was trained and evaluated using scenario-specific simulated data. Therefore, the reported localization performance does not represent clinical diagnostic accuracy. Future work will focus on realistic anatomical modeling, electrode contact effects, phantom validation, and experimental lower-leg measurements.

Keywords: Electrical Impedance Tomography, Frequency-Difference EIT, Physics-Informed Neural Network, Edema Detection, 3D Reconstruction

1. Introduction

Electrical Impedance Tomography (EIT) is a non-invasive imaging method that estimates internal conductivity from applied currents and boundary voltage measurements. Because it is low-cost, portable, radiation-free, and suitable for repeated monitoring, EIT has been studied in biomedical and industrial applications such as pulmonary monitoring, thromboembolic disease assessment, and multiphase flow imaging [1], [2]. However, EIT reconstruction is severely ill-posed and nonlinear, so measurement noise, modeling errors, and electrode uncertainty can significantly reduce image quality and spatial accuracy [3].

One difficult application is the early detection of subcutaneous edema. Edema changes tissue conductivity through abnormal interstitial fluid accumulation, but in the early stage these changes are usually small, diffuse, and weak in contrast. As a result, they are difficult to identify with standard reconstruction methods, especially when smoothness-based regularization blurs anomaly boundaries [3] [4]. Earlier studies have shown that impedance-based imaging can reflect fluid-related tissue changes, and lower-leg EIT assessment has demonstrated the feasibility of monitoring interstitial fluid variation in anatomically relevant

* *Corresponding author*

regions [5].

For this problem, Frequency-Difference Electrical Impedance Tomography (FD-EIT) is especially useful because it emphasizes conductivity-related change through differential measurements rather than relying only on absolute reconstruction. By comparing voltage responses from different conductivity states or excitation frequencies, FD-EIT can reduce common background effects and improve sensitivity to subtle tissue variation [2]. A 3D formulation is also important, since subcutaneous edema in the lower leg is inherently volumetric and varies with depth, circumferential position, and axial extent. Previous work has shown that 3D EIT provides more informative spatial characterization than simplified 2D models, although with greater computational complexity [6]. More recent learning-based studies have also shown that dedicated 3D approaches can improve reconstruction robustness and image quality [7]. Most conventional EIT reconstruction methods rely on regularized inverse solvers together with finite element modeling. Tikhonov regularization remains a common baseline because it is mathematically well understood, efficient, and straightforward to implement [3]. Its limitation is that smoothing can blur conductivity boundaries and reduce the visibility of localized anomalies, which is not ideal for subtle edema detection. Edge-preserving approaches such as total variation regularization have therefore been explored, although Tikhonov regularization remains a strong baseline for comparison [4].

In recent years, deep learning has also been explored for EIT reconstruction. Fan and Ying showed that neural networks can model both forward and inverse mappings in EIT, highlighting the potential of learning-based reconstruction for both 2D and 3D problems [8]. More recently, physics-aware methods have become important because they combine data-driven flexibility with physical consistency. Physics-Informed Neural Networks (PINNs), originally developed for forward and inverse PDE-constrained problems, embed governing equations directly into the training loss [7] [8].

This makes them attractive for EIT, where the physics is known but measurement data are often limited. EIT-specific studies have extended this idea through hybrid approaches, including two-stage CNN–PINN reconstruction and CPFI-EIT for non-smooth conductivity fields [7], [9]. Related work in current density impedance imaging and recent PINN-based EIT sensing studies also suggests that physics-informed learning is a promising alternative to classical reconstruction methods [10], [11]. At the same time, PINNs still face challenges such as optimization difficulty, sensitivity to sampling strategy, and reduced performance for irregular or high-frequency spatial features, which has motivated improved variants such as gradient-enhanced PINNs and adaptive sampling methods [12].

Motivated by these challenges, this paper presents a computational framework for early subcutaneous edema detection using 3D FD-EIT in a lower-leg model. A 3D domain with an appropriate electrode configuration is used to simulate boundary voltages, generate differential measurements, and define irregular edema-like anomaly scenarios. Two reconstruction approaches are then studied: a conventional Tikhonov-regularized baseline and a PINN-based conductivity reconstruction method. Their performance is compared under the identical synthetic conditions through qualitative and quantitative analysis of reconstructed conductivity fields, reconstruction errors, and anomaly localization behavior. To avoid limiting the evaluation to a single anomaly instance, the study considers a broader set of synthetic edema scenarios designed to reflect variation in spatial extent, shape irregularity, conductivity contrast and measurement noise.

Although learning-based and physics-informed reconstruction methods have been investigated for general EIT imaging, relatively limited attention has been given to early subcutaneous edema localization using a 3D lower-leg FD-EIT configuration. The present study does not claim to introduce a fundamentally new PINN architecture; rather, its contribution is the integration of a lower-leg 3D FD-EIT simulation framework, irregular edema-oriented conductivity scenarios, Tikhonov baseline reconstruction, and PINN-based reconstruction within a controlled comparative evaluation. This application-specific framework provides a reproducible computational basis for assessing whether physics-informed reconstruction can improve edema localization compared with a conventional regularized inverse solution.

2. Methodology

The proposed framework begins with the construction of a controlled 3D lower-leg computational domain and a corresponding finite element mesh. 16 electrodes are arranged on the outer surface of the model, and a forward EIT solver is used to generate voltage measurements for adjacent stimulation patterns. Two conductivity states are then simulated to obtain frequency-difference voltage data. A region-based synthetic edema domain is defined for inverse reconstruction, and irregular edema-like anomalies are introduced under a broader set of synthetic conditions. These conditions vary the anomaly morphology and reconstruction difficulty through differences in spatial extent, shape irregularity, conductivity contrast, and measurement noise. Conductivity reconstruction is then performed using two methods: a Tikhonov-regularized baseline and a PINN-based model. Finally, the reconstructed conductivity fields are compared using visualization, localization masks, and numerical evaluation metrics. The same 3D geometry, electrode arrangement, stimulation strategy and evaluation procedure are maintained throughout so that the comparative differences arise from anomaly conditions and reconstruction methods rather than from changes in acquisition setup.

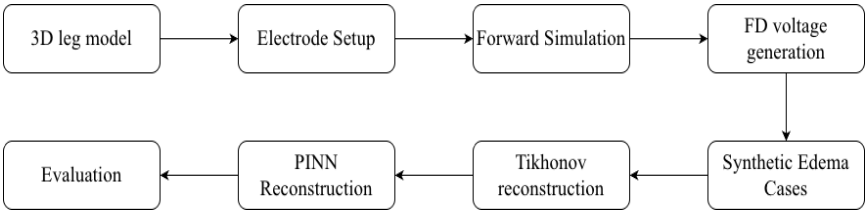

Figure 1. Workflow of 3D FD-EIT reconstruction framework

3. 3D leg geometry and electrode configuration

The computational domain represents a human lower limb as a 3D volume obtained by extruding an approximately elliptical cross-section along the axial direction. The model includes the main anatomical layers in simplified form, such as bone, muscle, fat, skin, and the subcutaneous region of interest, where edema-related conductivity changes are expected to occur. The domain is discretized using a tetrahedral finite element mesh, resulting in approximately 2087 nodes and 9179 elements. This mesh density provides a practical balance between numerical accuracy and computational cost, particularly for forward simulation and Jacobian-related calculations.

A set of 16 electrodes is placed on the outer surface of the leg model in a ring configuration around the mid-plane. Each electrode is represented as a tagged boundary surface, which allows the solver to apply current injection and extract electrode voltages programmatically. This arrangement forms the basis for adjacent current stimulation and voltage measurement in the proposed 3D FD-EIT framework.

Figure 2. 3D leg mesh, electrode tagged boundary view

4. Forward model and FD-EIT simulation

A stable 3D forward solver for EIT was developed on the constructed lower-leg mesh with 16 boundary electrode segments. Using adjacent electrode stimulation, one electrode pair was used for current injection and withdrawal while the remaining electrodes were treated as measurement electrodes. Under the quasi-static EIT assumption, the electrical potential inside the conductive domain satisfies the governing equation:

$$\nabla \cdot \left(\sigma(\mathrm{x})\nabla u(\mathrm{x})\right) = 0 \quad \text{in x} \in \Omega \qquad \text{(Equation 1)}$$

Where Ω denotes the 3D conductive domain, $\sigma(x)$ denotes the conductivity distribution and $u(x)$ is the electric potential. On the boundary, electrode regions enforce current constraints such that the net injected current over all electrodes remains zero. The finite element solution of (1) produces the spatial potential field within the domain, from which electrode voltages are obtained by surface averaging over each tagged electrode region. The computed results for all stimulation patterns form a full 16×16 voltage dataset. The simulated voltage response for stimulation pattern 0 shows smooth variation of boundary potentials across electrode indices with physically consistent relative differences, confirming the numerical stability of the forward solver.

Frequency-difference EIT simulations were then performed by generating two complete sets of electrode voltage measurements corresponding to two conductivity states representing different excitation conditions. Let $V(1)$ and V(2) denote the two voltage matrices. The FD-EIT response is obtained as

$$\Delta V = V^{(2)} - V^{(1)} \qquad \text{(Equation 2)}$$

Where ΔV represents the differential voltage dataset. This operation emphasizes conductivity-dependent changes while suppressing common-mode components. The voltage-difference pattern and FD response confirm a stable measurable differential response, demonstrating that the developed 3D pipeline can reliably generate synthetic FD-EIT datasets for subsequent inverse reconstruction experiments.

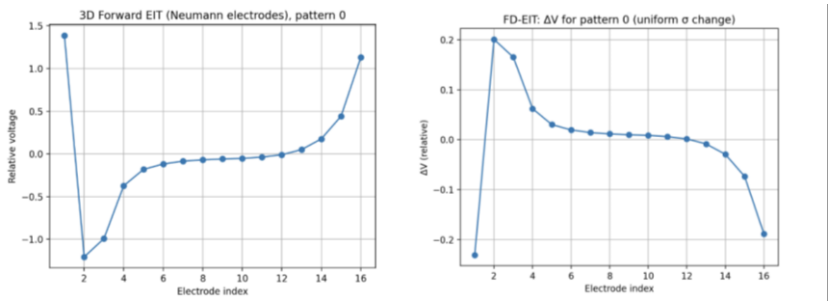

Figure 3. Forward-simulation voltage pattern for stimulation pattern 0, corresponding FD-EIT voltage-difference response

5. Synthetic edema modeling and reconstruction domain

To reduce the dimensionality of the inverse problem while preserving three-dimensional structure, conductivity reconstruction was performed on a region-based domain rather than at every mesh node. The reconstruction space was discretized along the circumferential, axial, and radial directions, and one conductivity value was assigned to each region. The total number of reconstruction regions is given by

$$N = N_\theta N_z N_r = 16 \times 8 \times 2 = 256 \qquad \text{(Equation 3)}$$

where $N\theta$, Nz and Nr are the numbers of angular, axial, and radial divisions, respectively. In this study $N\theta$=16, Nz = 8 and Nr =2, resulting in N = 256 reconstruction regions.

The background conductivity of normal tissue was assigned to be spatially uniform reference conductivity $\sigma_{\text{background}} = 1.0$ and whereas edema regions were assigned a higher conductivity value, $\sigma_{\text{edema}} = 1.28\ to\ 1.42$ depending on the synthetic scenario. Irregular edema-like conductivity distributions were generated within the 256-region reconstruction domain. The scenarios vary anomaly size, shape irregularity, conductivity contrast, and measurement noise. For each case, the ground-truth mask, conductivity field, and synthetic FD-EIT measurements were generated using the same region-based parameterization, enabling fair comparison between Tikhonov and PINN reconstruction.

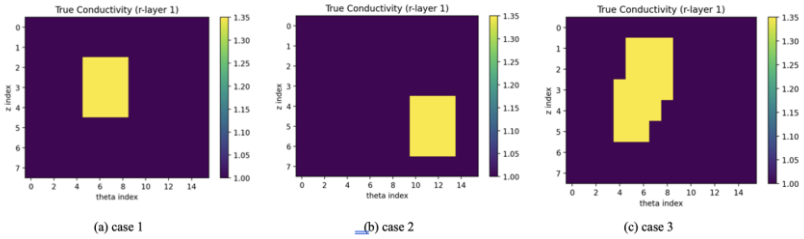

Figure 4. Ground-truth Conductivity of edema for different scenario edema

Table 1 Synthetic Edema Scenario Design summary

Case ID	Description	N_blobs	Radius range	Shape noise	Sigma edema	Measurement Noise
1	Very small compact	2	(0.12, 0.20)	0.03	1.32	0.03
2	Small compact	2	(0.15, 0.24)	0.04	1.35	0.05
3	Medium irregular	3	(0.18, 0.30)	0.05	1.35	0.05
4	Medium dense	3	(0.20, 0.34)	0.05	1.38	0.05
5	Large irregular	4	(0.24, 0.38)	0.06	1.35	0.05
6	Large spread	4	(0.26, 0.42)	0.07	1.4	0.06
7	Noisy low-contrast	3	(0.16, 0.30)	0.06	1.3	0.08
8	Fragmented irregular	5	(0.12, 0.26)	0.08	1.36	0.07
9	Large smooth high-contrast	2	(0.28, 0.46)	0.04	1.42	0.04
10	Hardest mixed case	4	(0.18, 0.36)	0.09	1.28	0.1

6. Baseline reconstruction using Tikhonov regularization

As a conventional inverse solution, Tikhonov regularization was used as the baseline method for conductivity reconstruction. Let Δv denote the differential boundary-voltage measurement vector and J the sensitivity (Jacobian) matrix relating conductivity changes to voltage changes. Under the linearized FD-EIT model, the measurement equation is written as

$$\Delta \mathrm{v} = \mathrm{J}\,\Delta\sigma \qquad \text{(Equation 4)}$$

where Δσ is the unknown conductivity-change vector over the reconstruction regions. Because the inverse problem is ill-posed, the conductivity change was estimated by minimizing the Tikhonov objective

$$\Delta\sigma_{\mathrm{Tik}} = \underset{\Delta\sigma}{\operatorname{argmin}}(\| \mathrm{J}\Delta\sigma - \Delta \mathrm{v} \|_2^2 + \lambda \| \Delta\sigma \|_2^2), \qquad \text{(Equation 5)}$$

where λ is the regularization parameter. The corresponding closed-form solution is

$$\Delta\sigma_{\mathrm{Tik}} = (\mathrm{J}^T\mathrm{J} + \lambda \mathrm{I})^{-1}\mathrm{J}^T\Delta \mathrm{v} \qquad \text{(Equation 6)}$$

Here, J is the sensitivity matrix, Δv is the measured differential voltage vector, λ is the regularization parameter, and I is the identity matrix. In this study, λ=0.1 was used for all evaluated scenarios. The reconstructed conductivity field was then obtained by adding the estimated conductivity change to the background conductivity:

$$\sigma_{\mathrm{Tik}} = \sigma_{\mathrm{bg}} + \Delta\sigma_{\mathrm{Tik}} \qquad \text{(Equation 7)}$$

where the background conductivity was set to $\sigma_{\mathrm{bg}} = 1.0$. To assess anomaly localization, the reconstructed conductivity field was converted into a binary edema mask using a midpoint threshold between the background and edema conductivities:

$$\tau = \frac{\sigma_{\mathrm{bg}} + \sigma_{\mathrm{edema}}}{2} \qquad \text{(Equation 8)}$$

and then the mask rule:

$$m_i = \begin{cases} 1, & \hat{\sigma}_i \geq \tau \\ 0, & \hat{\sigma}_i < \tau \end{cases} \qquad \text{(Equation 9)}$$

A region was classified as edema if $\sigma_{\text{Tik, i}} \geq \tau$, and as background otherwise. Since the synthetic scenarios used edema conductivity values in the approximate range 1.28 to 1.42, the threshold varied accordingly across scenarios. The Tikhonov method provides a stable and interpretable baseline, but its smoothing effect often leads to diffuse anomaly boundaries and less localized reconstructions, especially under irregular or more challenging edema conditions. Representative baseline reconstructions are shown in the corresponding figure and are later compared with the PINN-based results using quantitative error and localization metrics.

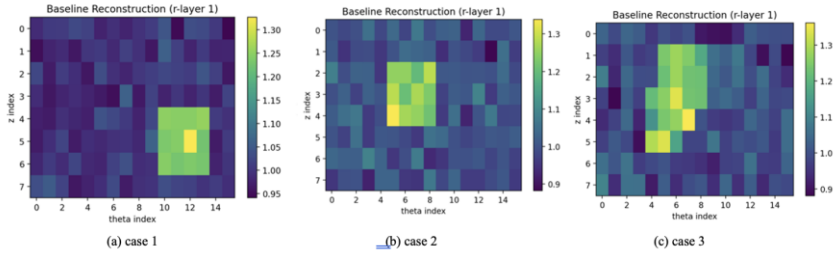

Figure 5. Baseline Tikhonov reconstructions at radial layer 1 for different position edema

7. PINN architecture and composite loss

The PINN was implemented as a multilayer perceptron that maps the normalized spatial coordinate of each reconstruction region to its conductivity change. The network predicts

$$\Delta\sigma_{\text{pred}} = f_\theta(x_i) \qquad \text{(Equation 10)}$$

where $\mathbf{x}_i = (x_i, y_i, z_i)$ denote the normalized coordinate of region i, f_θ is the neural network with learnable parameters θ. The corresponding absolute conductivity prediction is then

$$\hat{\sigma}_i = \sigma_{\text{bg}} + \Delta\hat{\sigma}_i$$

where $\sigma_{\text{bg}} = 1.0$. The network used a 3-dimensional input, several fully connected hidden layers with tanh activation, and a scalar output for conductivity-change prediction. This architecture is simple enough for stable training in the region-based domain while remaining expressive enough to represent irregular edema patterns. Each training sample corresponded to one reconstruction region, and the full conductivity field was obtained by evaluating the network over all N=256 regions.Training was performed separately for each synthetic edema scenario using a composite loss so that the predicted conductivity field satisfied both reconstruction and structural requirements. The supervised conductivity loss was defined as

$$\mathcal{L}_{\text{sup}} = \frac{1}{N}\sum_{i=1}^{N}\left(\Delta\sigma_{\text{pred},i} - \Delta\sigma_{\text{true},i}\right)^2 \qquad \text{(Equation 11)}$$

where $\Delta\sigma_i^{\text{true}}$ is the true conductivity change at region i. To enforce measurement consistency, the predicted differential voltage was computed as

$$\Delta\hat{\mathrm{v}} = \mathrm{J}\,\Delta\hat{\sigma},$$

and the data loss was written as

$$\mathcal{L}_{\text{data}} = \frac{1}{M}\|\Delta\hat{\mathrm{v}} - \Delta\mathrm{v}\|_2^2 \qquad \text{(Equation 12)}$$

where J is the sensitivity matrix, $\Delta\mathbf{v}$ is the measured differential voltage vector and M is the number of differential voltage measurements. A smoothness penalty was added over neighboring regions:

$$\mathcal{L}_{\text{smooth}} = \frac{1}{|E|}\sum_{(i,j)\in E}\left(\Delta\hat{\sigma}_i - \Delta\hat{\sigma}_j\right)^2 \qquad \text{(Equation 13)}$$

E is the set of neighboring region pairs. To weakly incorporate information from the baseline reconstruction, a guidance term was also used:

$$\mathcal{L}_{\text{prior}} = \frac{1}{N}\sum_{i=1}^{N} w_i \left(\Delta\hat{\sigma}_i - \Delta\sigma_i^{\text{base}}\right)^2 \quad \text{(Equation 14)}$$

where $\Delta\sigma_i^{\text{base}}$ is the baseline conductivity-change estimate and w_i is a spatial guidance weight. The total loss was defined as

$$\mathcal{L}_{\text{total}} = \lambda_{\text{sup}}\mathcal{L}_{\text{sup}} + \lambda_{\text{data}}\mathcal{L}_{\text{data}} + \lambda_{\text{smooth}}\mathcal{L}_{\text{smooth}} + \lambda_{\text{prior}}\mathcal{L}_{\text{prior}} \quad \text{(Equation 15)}$$

In this study, the loss weights were set to

$$\lambda_{\text{sup}} = 1.0, \quad \lambda_{\text{data}} = 1.0, \quad \lambda_{\text{smooth}} = 0.05, \quad \lambda_{\text{prior}} = 0.1 \quad \text{(Equation 16)}$$

Table 2 PINN Training Configuration

Parameter	Value / Description
Input	Normalized region coordinates (x, y, z)
Output	Predicted conductivity change Δσpred
Network	Fully connected multilayer perceptron
Hidden layers	4
Activation	Tanh
Optimizer	Adam
Learning rate	1 x 10^{-3}
Epoch	1200
Loss terms	Supervised, measurement consistency, smoothness, prior guidance
Training mode	Full-batch training; trained separately for each synthetic case

The loss weights were chosen based on observing the relative sizes of the individual loss components during early training. The same weights were used in all scenarios to make sure the comparisons were fair. This formulation allows the model to balance direct conductivity learning, measurement agreement, spatial regularity, and baseline-guided stabilization within a unified reconstruction framework.

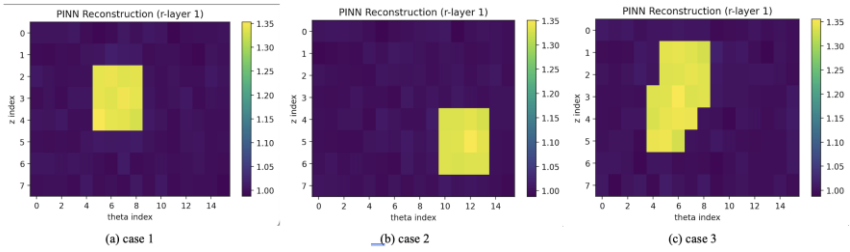

Figure 6. PINN reconstruction for different scenario edema

For each synthetic case, the PINN was trained separately using the same architecture and loss formulation. After convergence, the best checkpoint was evaluated over all 256 reconstruction regions to obtain the conductivity-change field, which was converted to absolute conductivity and compared with the ground truth and Tikhonov baseline.

8. Edema localization and comparative evaluation

Because the ultimate goal is anomaly localization, the conductivity reconstruction was converted into a binary edema map. A threshold was defined midway between the background and edema conductivity values, and the predicted edema mask was obtained by thresholding the reconstructed conductivity field. The same approach was also applied to the baseline reconstruction so that both methods could be compared fairly at the localization level. The framework was evaluated using both reconstruction-accuracy and localization-quality metrics. The reconstruction accuracy and localization quality were evaluated using Root Mean Square Error (RMSE), Mean Absolute Error (MAE), Relative Error, and Dice Score. The RMSE and Dice Score may be written as

$$\mathrm{RMSE} = \sqrt{\frac{1}{N}\sum_{i=1}^{N}\left(\sigma_{\mathrm{pred},i} - \sigma_{\mathrm{true},i}\right)^2} \quad \text{(Equation 17)}$$

$$\mathrm{MAE} = \frac{1}{N}\sum_{i=1}^{N}\left|\sigma_{\mathrm{pred},i} - \sigma_{\mathrm{true},i}\right| \quad \text{(Equation 18)}$$

$$\text{Relative Error} = \frac{\| \sigma_{\mathrm{pred}} - \sigma_{\mathrm{true}} \|_2}{\| \sigma_{\mathrm{true}} \|_2} \quad \text{(Equation 19)}$$

$$\mathrm{Dice} = \frac{2\left|m_{\mathrm{pred}} \cap m_{\mathrm{true}}\right|}{\left|m_{\mathrm{pred}}\right| + \left|m_{\mathrm{true}}\right|} \quad \text{(Equation 20)}$$

where, $\sigma_{\mathrm{pred},i}$ and $\sigma_{\mathrm{true},i}$ denote predicted and true conductivity values and m_{pred} and m_{true} denote the predicted and true edema masks. Comparison was performed using visual conductivity maps, error maps, edema-mask overlap, and numerical metrics under identical synthetic conditions. The results indicate that the PINN yields a more localized and structured anomaly reconstruction than the Tikhonov baseline, while the baseline remains a stable and interpretable reference solution.

Table 3 Case-wise quantitative comparison

Case ID	Baseline RMSE	PINN RMSE	Baseline MAE	PINN MAE	Baseline Relative Error	PINN Relative Error	Baseline Dice	PINN Dice
1	0.0571	0.0142	0.0436	0.0111	0.0551	0.0137	0.8936	1
2	0.0794	0.0225	0.0636	0.018	0.0754	0.0213	0.875	1
3	0.0815	0.0225	0.0618	0.0177	0.0766	0.0212	0.8649	1
4	0.0864	0.0228	0.0665	0.0176	0.0801	0.0212	0.9302	1
5	0.089	0.0226	0.0676	0.0179	0.0818	0.0207	0.8544	1
6	0.1161	0.0276	0.0914	0.0222	0.1043	0.0248	0.8421	1
7	0.0961	0.0348	0.0755	0.0272	0.0908	0.0329	0.6905	1
8	0.106	0.0316	0.0823	0.0248	0.0979	0.0292	0.7473	1
9	0.1057	0.0203	0.0822	0.0161	0.0951	0.0183	0.835	1
10	0.1127	0.0431	0.088	0.0342	0.1064	0.0407	0.6154	1

Table 4 overall summary statistics

Metric	Baseline Mean ± Std	PINN Mean ± Std	Improvement
RMSE	0.0930 ± 0.0180	0.0262 ± 0.0083	71.83%
MAE	0.0723 ± 0.0145	0.0207 ± 0.0066	71.38%
Relative Error	0.0863 ± 0.0157	0.0244 ± 0.0079	71.74%
Dice Score	0.8148 ± 0.0990	1.0000 ± 0.0000	18.52%

The results show that the PINN-based method consistently outperformed the Tikhonov baseline across all ten edema scenarios. Lower RMSE, MAE, and relative error values indicate that the PINN reconstructed the conductivity distribution more accurately, while the higher Dice scores show better localization of the edema region. The Dice score of 1.0000 obtained by the PINN in all cases should be interpreted within the controlled synthetic setting of this study, where both training and evaluation were performed on scenario-specific simulated data. Therefore, the Dice score reflects complete mask overlap under this synthetic thresholding setup and should not be interpreted as perfect edema detection in experimental or clinical conditions. Overall, the findings suggest that the proposed PINN framework provides more localized and structurally consistent reconstructions than the baseline method for the considered 3D FD-EIT edema cases.

9. Discussion

The region-based reconstruction domain reduces computational cost by estimating conductivity over 256 regions rather than all mesh elements, while still preserving the 3D structure of the lower-leg model. The more difficult cases, especially the noisy low-contrast and hardest mixed scenarios, indicate that further robustness testing under broader noise levels and experimental measurements is necessary. The results show that the PINN-based method produced lower reconstruction error and more localized edema patterns than the Tikhonov baseline. This improvement can be attributed to the composite loss formulation, which combines supervision of conductivity, measurement consistency, spatial smoothness, and weak prior guidance. In contrast, Tikhonov regularization stabilizes the inverse problem but tends to oversmooth localized conductivity changes. The main limitation of this study is that all evaluations were performed using synthetic data. Real FD-EIT measurements may be affected by electrode contact impedance, anatomical variability, motion artifacts, hardware noise, and tissue-property uncertainty. Therefore, the present results should be interpreted as computational feasibility evidence only. Future work will include realistic anatomical modeling, phantom experiments, and validation using experimental or clinical lower-leg measurements.

10. Conclusion

This paper presented a 3D FD-EIT framework for early subcutaneous edema detection using Tikhonov regularization and PINN-based conductivity reconstruction. Under controlled synthetic scenarios, the PINN reduced reconstruction error and produced more localized edema masks than the Tikhonov baseline. The Dice score of 1.0 reflects threshold-based overlap with predefined synthetic masks and should not be interpreted as clinical detection performance. Future work will focus on realistic anatomical modeling, electrode contact effects, phantom validation, and experimental lower-leg measurements.

References

[1] B. H. Brown, "Electrical impedance tomography (EIT): A review," Journal of Medical Engineering & Technology, vol. 27, no. 3, pp. 97-108, 2003.

[2] J. P. Leitzke and H. Zangl, "A review on electrical impedance tomography spectroscopy," Sensors, vol. 20, no. 18, pp. 51-60, 2020.

[3] B. Jin and P. Maass, "An analysis of electrical impedance tomography with applications to Tikhonov regularization," ESAIM: Control, Optimisation and Calculus of Variations, vol. 18, no. 4, pp. 1027-1048, 2012.

[4] A. Borsic, B. M. Graham, A. Adler and Lionheart, "In vivo impedance imaging with total variation regularization," IEEE Transactions on Medical Imaging, vol. 29, no. 1, pp. 44-54, 2010.

[5] B. Grychtol, B. Müller and A. Adler, "3D EIT image reconstruction with GREIT," Physiological Measurement, vol. 37, no. 6, pp. 785-800, 2016.

[6] R. Ogawa, M. R. Baidillah, S. Akita and M. Takei, "Investigation of physiological swelling on conductivity distribution in lower leg subcutaneous tissue by electrical impedance tomography," Journal of Electrical Bioimpedance, vol. 11, no. 1, pp. 19-25, 2020.

[7] Z. Yi, Zhou Chen and Yunjie Yang, "A Learning-Based 3D EIT Image Reconstruction Method," International Conference of Bioelectromagnetism, Electrical Bioimpedance, and Electrical Impedance Tomography, 2022.

[8] Y. Fan and L. Ying, "Solving Electrical Impedance Tomography with Deep Learning," Journal of Computational Physics, vol. 404, 2019.

[9] M. Raissi, P. Perdikaris and G. Karniadakis, "Physics-informed neural networks: A deep learning framework for solving forward and inverse problems involving nonlinear partial differential equations," Journal of Computational Physics, vol. 378, pp. 686-707, 2019.

[10] C. Duan, J. Huang, Y. Jiao, X. Lu and J. Z. Yang, "Current density impedance imaging with PINNs," Journal of Computational and Applied Mathematics, vol. 452, 2024.

[11] D. Smyl, T. N. Tallman, L. Homa, C. Flournoy, S. J. Hamilton and J. Wertz, "Physics Informed Neural Networks for Electrical Impedance Tomography," Neural Networks, vol. 188, 2025.

[12] X. Yang, Y. Zhang, H. Chen, G. Ma and X. Wang, "A two-stage imaging framework combining CNN and physics-informed neural networks for full-inverse tomography: A case study in electrical impedance tomography," IEEE Signal Processing Letters, vol. 32, 2024.